PHYSICS AND CHEMISTRY OF SOLID STATE
V. 22, No. 1 (2021) pp. 132-140
Section: Chemistry

DOI: 10.15330/pcss.22.1.132-140

Vasyl Stefanyk Precarpathian National University

ФІЗИКА І ХІМІЯ ТВЕРДОГО ТІЛА
Т. 22, № 1 (2021) С. 132-140
Хімічні науки

PACS: 81.05.U; 78.67.Sc ISSN 1729-4428

K. Karthik[1], D. Radhika[2], D. Gnanasangeetha[3], K. Gurushankar[4,5], Md Enamul Hoque[6]

Two-Dimensional Based Hybrid Materials for Photocatalytic Conversion of Carbon Dioxide into Hydrocarbon Fuels: a Mini Review

[1]*School of Advanced Materials Science and Engineering, Kumoh National Institute of Technology, 61 Daehak-ro, Gumi-si, Gyeongbuk, Republic of Korea, karthikkannanphotochem@gmail.com*
[2]*Department of Chemistry, Faculty of Engineering and Technology, Jain-Deemed to be University, Jakkasandra, Ramnagara, Karnataka, India, radhikadv8@gmail.com*
[3]*Department of Chemistry, PSNA College of Engineering and Technology, Dindigul, Tamil Nadu, India, sangithprakash@psnacet.edu.in*
[4]*Higher Medical and Biological School, South Ural State University, Chelyabinsk, Russia.*
[5]*Department of Physics, School of Advanced Sciences, Kalasalingam Academy of Research and Education, Krishnankoil, Virudhunagar, Tamilnadu, gurushankar01051987@gmail.com*
[6]*Department of Biomedical Engineering, Military Institute of Science and Technology (MIST), Mirpur Cantonment, Dhaka, Bangladesh, enamul1973@gmail.com*

Carbon dioxide conversion to chemicals and fuels based on two-dimensional based hybrid materials will present a thorough discussion of the physics, chemistry, and electrochemical science behind the new and important area of materials science, energy, and environmental sustainability. The tremendous opportunities for two-dimensional based hybrid materials in the photocatalytic carbon dioxide conversion field come up from their huge number of applications. In the carbon dioxide conversion field, nanostructured metal oxide with a two-dimensional material composite system must meet assured design and functional criteria, as well as electrical and mechanical properties. The whole content of the proposed review is anticipated to build on what has been learned in elementary courses about synthesizing two-dimensional nanomaterials, metal oxide with composites, carbon dioxide conversion requirements, uses of two-dimensional materials with nanocomposites in carbon dioxide conversion as well as fuels and the major mechanisms involved during each application. The impact of hybrid materials and synergistic composite mixtures which are used extensively or show promising outcomes in the photocatalytic carbon dioxide conversion field will also be discussed.

Keywords: 2D nanomaterials; characterization; photocatalytic carbon dioxide conversion; fuels.

Received 3 February 2021; Accepted 5 March 2021.

Introduction

The severe environmental issues like the greenhouse effect and climate transform due to significantly rising meteorological carbon dioxide (CO_2) level (via ignition of vestige fuel, desertification, and person stimulates). Additionally, energy utilization is likely to attain around 2 times the present energy utilization by 2050. To overcome these problems and reduce the meteorological CO_2 concentration via the conversion of CO_2 can be utilized to decrease the CO_2 emission and into hydrocarbon fuels. Moreover, CO_2 is a gorgeous preliminary precursor material for generating chemical energy, because of its profusion, economical, and less toxicity. Owing to its solidity, additional energy is supported to convert CO_2 into hydrocarbon or chemical fuels. Diverse methods have been utilized for CO_2 transformation which comprises thermal, chemical, photocatalytic, electrocatalytic, and biological conversion. Amid such techniques, the photocatalytic

and electrocatalytic in CO_2 conversion acts as a noteworthy function to determine energy disaster and global warming. The development pays the photocatalytic (light-driven) and electrocatalytic alternation of CO_2 to value-added chemical fuels (methane: CH_4, carbon monoxide: CO, formaldehyde: CH_2O, methanol: CH_3OH, and ethanol: C_2H_5OH) [1-4].

For this process to suit cheaply feasible, dissimilar scientifically progress have to be prepared. Modern works determined on discovering dissimilar catalysts and products that can be fabricated. Diverse categories of catalysts that can catalyze the CO_2 reduction reaction (CRR) have been produced and investigated. Transition metals (Pt, Pd, Rh, Ag, Au, and Ni), oxides (ZnO, NiO, CuO, CeO_2, TiO_2, RuO_2, and SnO_2, etc.), carbides, chalcogenides, and metal-organic frameworks have revealed possible as catalysts for CRR [5, 6].

Recently, 2D hybrid materials have earned wide-ranging notice as an electrode for diverse purposes such as batteries, proton reduction, oxygen reduction, and fuel cells. 2D hybrid materials have a large surface area, carrier mobility, thermal conductivity, and current and heat conduction. Graphene displays several exclusive properties, which comprise a tremendously huge theoretical specific surface area (2630 $m^2 g^{-1}$), excellent optical transparency (~ 97.7 %), as well as elevated mechanical strength (1 TPa) and thermal conductivity (~ 5000 $Wm^{-1} K^{-1}$) [7]. Graphene-based nanocomposites exhibit various purposes in the field of photocatalysis, electrochemical devices, energy storage, and conversion systems, etc. Particularly, Graphene-based nanocomposites showed impending performance in the CRR owing to its tremendous conductivity and absorption capability [8, 9]. MXenes, an original 2D transition metal carbides, and nitrides have newly fascinated important consideration and 2D MXene layers are typically fabricated via eradicating the "A" group layers from the MAX layered phase with hydrofluoric acid (HF), which produces diverse terminal functional groups (-O, -OH, and -F) on the surface. Owing to their outstanding electrical conductivity, elemental composition adjustability, and convenient surface functional groups, MXenes have exposed huge impending in numerous appliance fields (hydrogen evolution, oxygen evolution, and oxygen reduction reactions). Importantly, MXenes also demonstrate incredible impending in the CRR [10].

Furthermore, 2D-based (Graphene and MXene) nanomaterials with distinct morphology also participate in a significant function in their performance toward CRR. The overall CRR efficiency can be improved via the fabrication of efficient 2D-based hybrid nanomaterials (catalyst). Plentiful reports have been dedicated to the preparation of metal oxide / composite catalysts for the CRR process. To develop the performance of catalyst material, dissimilar intensification strategies are obtainable which comprise composite with 2D based nanomaterials [11].

In this review, the various 2D-based hybrid materials (catalysts) for CO_2 conversion are summarized. Additionally, the influence of various 2D-based hybrid catalytic materials and photocatalytic conversion technique for CO_2 conversion is described with applications.

I. Synthesis of 2D-based nanocomposites

The preparation and assembly of 2D graphene/MXene-based nanocomposites offer persuasive research, mainly communicated to organize their morphology and properties for realistic purposes. In this part, we will spotlight on the fabrication of 2D graphene/MXene-based nanocomposites.

1.1 Fabrication of graphene oxide (GO) – Modified Hummers method

GO was fabricated by improved Hummers method [12]. In this, a 9:1 combination of concentrated H_2SO_4/H_3PO_4 (360:40 mL) was inserted to a combination of graphite flakes (3.0 g) and $KMnO_4$ (18.0 g), constructing a minor exotherm to 308 - 313 K. The solution was then heated to 323 K and stirred for 12 h and cooled to room temperature and transfered onto ice (400 mL) with 30 % H_2O_2 (3 mL). Then it was centrifuged (4000 rpm for 4 h). The solid material was cleaned with 200 mL of water, 30 % HCl, and ethanol. Then it was again washed with 200 mL of ether. The solid attained was dried at 60˚C overnight. The final product was labeled as graphene oxide (GO). Fig. 1 represents the general mechanism wherein graphite was first oxidized by improved Hummer's method and it was reduced by hydrothermal / chemical method finally reduced graphene oxide [13].

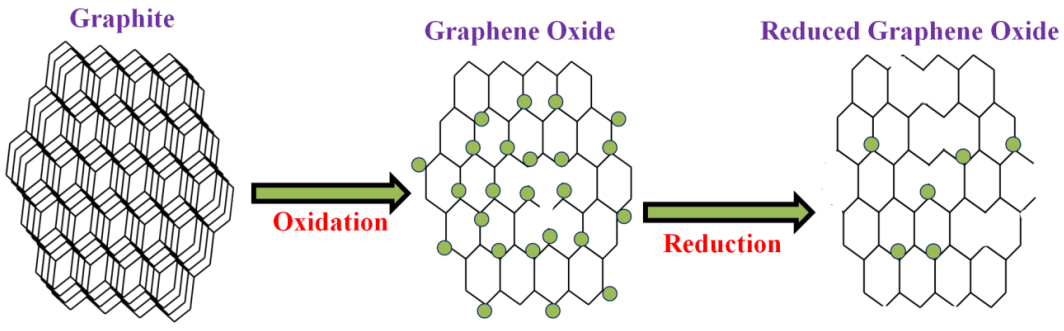

Fig. 1. Mechanism for the preparation of reduced graphene oxide from graphite.

1.2 Synthesis of reduced graphene oxide (rGO) – Hydrothermal method

The obtained graphene oxide (GO) from improved Hummers method was taken (100 mg) and mixed with ethanol (30 mL) and double distilled water (60 mL). This solution was sonicated for 4 h and autoclaved at 393 K for 12 h in a 100 mL autoclave bottle. The obtained solution was centrifuged at 4000 rpm with water and ethanol. Then the solid was dried at 333 K in an oven for overnight. The final product was named as rGO.

1.3 Preparation of TiO_2 nanocomposite with rGO (T0/rGO)– Hydrothermal method

The nanocomposite of TiO_2 NPs with rGO was fabricated by the hydrothermal method (Fig. 3). 0.01 g of GO and 0.1 g of TiO_2 NPs (T0) were added to the mixture of water (60 mL) and ethanol (30 mL). The solution was sonicated for 4 h. Then it was autoclaved at 393 K for 12 h in a 100 mL autoclave bottle. Then it was centrifuged at 4000 rpm for 2 h. The product was dried at 333 K for 12 h. Then obtained solid was labeled as TO/rGO.

1.4 Synthesis of MXene

$Ti_3C_2T_x$ MXene fabrication: 2.0 g of Ti_3AlC_2 was gradually included to 40 mL of 40 % fluorhydric acid (HF) solutions and the reaction combination was combined using stirrer at 60 ºC for 18 hrs. The solid product was collected by centrifuge, cleaned with double distilled water, and lyophilized.

$$Ti_3AlC_2 + 3HF \rightarrow Ti_3C_2 + AlF_3 + 3/2H_2$$

$$Ti_3C_2 + 2\ H_2O \rightarrow Ti_3C_2\ (OH)_2 + H_2$$

$$Ti_3C_2 + 2\ HF \rightarrow Ti_3C_2F_2 + H_2$$

The preparation of all other MXene sheets Al-enclosing MAX phases, the above scheme was applied. Especially, the etching circumstances (HF concentration and time) are essential to modify a provided different MAX phase widely, controlled by the particle size and temperature. For instance, diminishing the MAX phase particle size by mechanical attrition can resourcefully decrease the crucial etching time and/or concentration of HF [14, 15]. Further, deviations in M-Al bond energies for disparate MAX phases also require dissimilar etching circumstances. For the case, In Ti_2AlC with superior Ti-Al correlated with Nb-Al bond energy in Nb_2AlC lead to enhanced concentration of HF and extensive etching time [16]. Hence, proper etching circumstances are mandatory to accomplish superior products and terminate the swap of MXenes from MAX phases. In recent times, the convention of NH_4HF_2 as an etchant in substitute for the destructive HF was reported by Hamil et al. [17]. Ghidiu et al. has illustrated the newest superior-yield procedure for the timely synthesis of plentiful MXene sheets [18].

Herein, Ti_3C_2Tx was prepared via dissolving Ti_3AlC_2 powders in solutions of HCl and LiF, then gave heating to the combination for 45 h at 40 ºC, and then washed the sediment to eradicate the resulted product and enhanced the pH. Furthermore, the preparation of diverse Ti_2CT_x morphology was attained currently through the specific surfactant, intercalating agent,. Though, many investigates are insisting in order to get a fine-synchronized morphology, imaginative sizes, construction, and also cessation cluster creation process.

II. Characterization of 2D based hybrid materials

2.1. Characterization of 2D graphene based nanocomposites

2.1.1 Structural and morphological analysis of 2D graphene based nanocomposites

The nanocomposite (NC) was synthesized by a low-temperature solution process. The XRD patterns of GO, Ce nanoparticles (CN), and the CN/GO NC are illustrated in Figure 2a. Figure 4a shows the crystalline structure of CN with the cubic crystal structure of CeO_2 (JCPDS 65-2975). XRD pattern of the CN/GO NC (Figure 4a) displays the crystalline structure of CN which validates the occurrence of CN in the prepared NC. It is revealing that the refractive index of the CN/GO composite with a sharper peak in relationship to that of CN, which is accredited to a greatly well-organized CN crystallinity in the NC. Alternatively, it is monitored that the distinctive XRD pattern of GO around 25° considerably decreases in the CN/GO NC, which is attention to be owing to the disorder of stacking of GO sheets in the NC [19].

In Fig. 2b showed the XRD pattern of the S-TiO_2/rGO (STR) NC with 5 % wt. (rGO), illustrates a smaller crystallinity degree of various anatase, in relation to the diffraction pattern of pristine anatase TiO_2, in addition to a change in peak locations, representing lattice defects provoked by the insertion of sulfur. The intensity diminish of crystallinity is noteworthy starting the worsening of the peaks in the STR diffraction pattern, i.e., the peak intensity of the (1 0 1) diminished and the peak has widened, while the planes of (1 0 3), (1 1 2), (1 0 5), and (2 1 1) *h k l* indices are hardly discernable [20].

The peaks materialized at 1352 and 1600 cm^{-1} due to the D-mode and G-mode respectively (Fig. 2c). The G-mode signifies the occurrence of residual functional groups (imperfect reduction of the initial material). Furthermore, the Raman intensities ratio (I_d/I_g) of ~ 1.4 was estimated. There is no vibrational mode detection for the anatase phase [20].

Fig 2d showed the Raman spectrum of the synthesized TiO_2 and TSFG samples. The TiO_2 anatase phase displayed attribute scatterings at 145, 393, and 638 cm^{-1} (Fig. 2d), while the TiO_2 rutile phase displayed distinctive scatterings at 445 (E_g). The mainly attention information that can be extracted from the Raman studies is that the position of the distinctive scatterings altered in the TSFG sample. Furthermore, no Raman peaks equivalent to SiO_2 can be examined; hence, either Si^{4+} displays in the changed locations in the TiO_2, or it is present as amorphous SiO_2. Peaks at 513 and 700 cm^{-1} can be featured to γ-Fe_2O_3, correspondingly. Furthermore for the sample of TSFG, both the D and G bands of GO usually positioned at 1323 and 1570 cm^{-1}, have moved to lower frequencies in relationship with GO (Fig. 2b). This is major confirmation that GO was

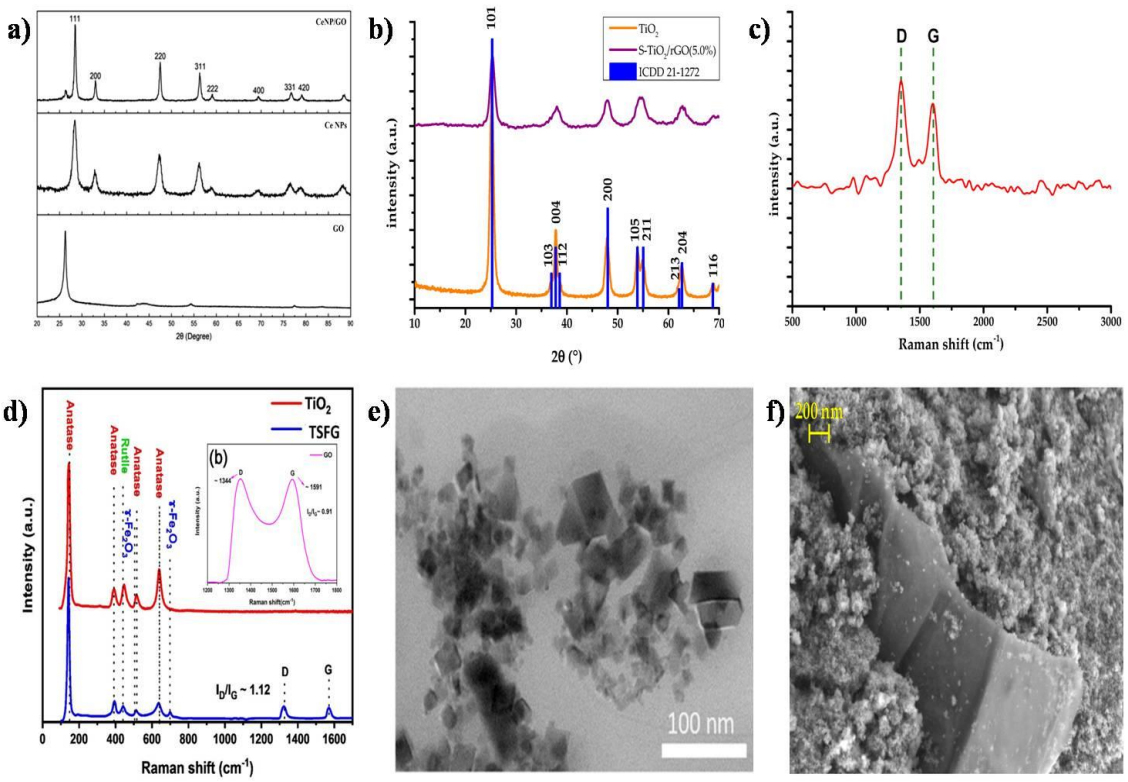

Fig. 2. XRD pattern of (a) CN/GO NC, (b) S-TiO_2/rGO NC, (c) Raman spectrum of S-TiO_2/rGO NC, (d) TiO_2 and TSFG, (e) TEM image of CN/GO NC and (f) SEM image of S-TiO_2/rGO NC. Reprinted with permission from [Ref. 19, 20, 21].

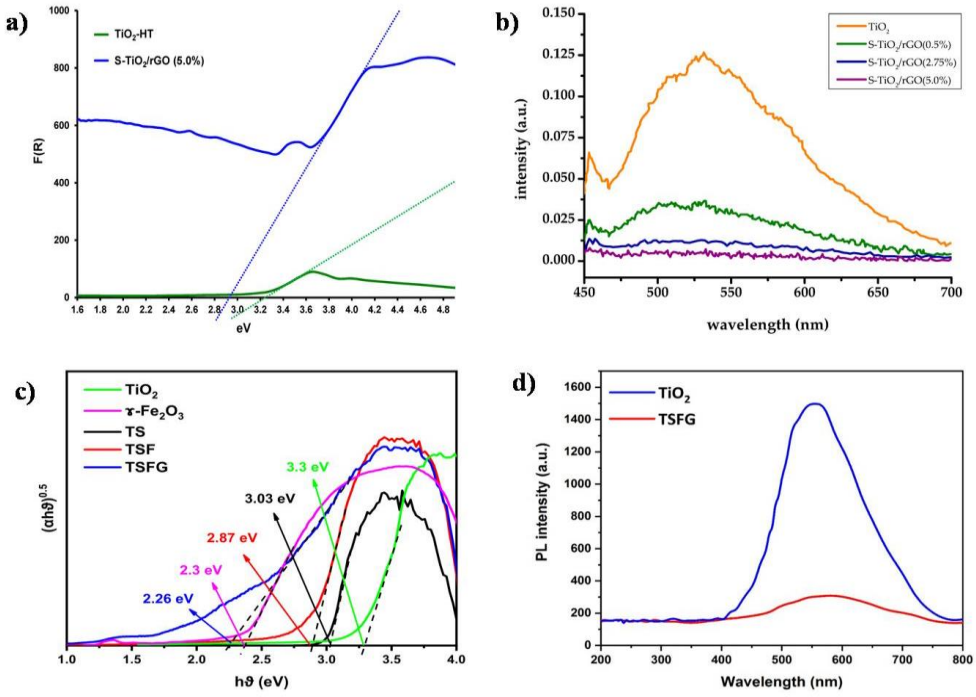

Fig. 3. (a) DRS spectra of TiO_2 and STR, (b) PL spectra of TiO_2 and STR composite, (c) optical energy bandgap of the synthesized samples and (d) PL spectra of TiO_2 and TSFG samples. Reprinted with permission from [Ref. 20, 21].

effectively reduced and was therefore present as rGO [21].

Figure 2e shows the bright-field TEM image of CN/GO composite. For the CN/GO NC, which is displayed in Figure 2e, CNs are homogeneously dispersed all over the GO sheets. Accordingly, it is validated that the low-temperature solution procedure can be fruitfully employed to fabricate the CN/GO NC [19]. In figure 2f, the SEM images of STR NC showed the collected TiO_2 particles are sandwiched with rGO

sheets. Nevertheless, such segment transport boundaries were renowned by other authors submitting related fabrication processes of the composites [20].

2.1.2 Optical properties of 2D graphene based nanocomposites

TiO_2 bandgap was established to be 3.21 eV (Fig. 3a), whereas the bandgap for the STR NC was 2.92 eV [20]. The decrease of the bandgap is due to the doping of sulfur and insertion rGO. Moreover, Wang et al. has reported similar bandgap for S-TiO_2, therefore S doping and rGO accomplish the same bandgap narrowing threshold [22].

In Figure 3b, shows the photoluminescence spectra of TiO_2, S-TiO_2/rGO NC with different concentrations. The doping of sulfur and rGO inclusion within the TiO_2 matrix exhibited more inhibition of charge recombination. TiO_2 demonstrated a peak at 531 nm which is equivalent to recombination electron and hole by surface adsorbed oxygen. The remarkable decrease of emission is due to the doping of sulfur and insertion rGO in the TiO_2 matrix. Liu et al. have reported the impurity levels can trap photo-generated charges by the sulfur doping, which is additional donated by insertion rGO performing as an electron-sink**.** Nevertheless, the quantity of rGO appears to be a vital role, as the counts of deliberated PL diminished with the quantity of rGO rising contained by the STR NC. Nevertheless, rising rGO (2.75 to 5 wt. %) from conveys deteriorating returns. The larger amount of rGO guides to a contradictory effect, i.e., enhance in recombination, as rGO can perform as a recombination center [20].

Figure 3c displays the direct bandgap values that were established by extrapolating the linear section of the Tauc's plot of $(\alpha h\upsilon)^{1/2}$ against the hυ. The bandgap for TiO_2 and γ-Fe_2O_3 is 3.3 and 2.3 eV, correspondingly. E_g was computed as 3.03 eV (TS) and 2.87 eV (TSF), validating the decrease in bandgap fabricated by the adding of γ-Fe_2O_3. Still, E_g is the least for the sample of TSFG (2.26 eV) [21].

Photoluminescence (PL) experiments were executed to inspect the recombination probability of bare TiO_2 and TSFG photocatalysts (Fig. 3d). The PL intensity of the TSFG photocatalyst was importantly lesser than that of the bare TiO_2. This could be communicated to the lesser e^-/h^+ recombination probability of the TSFG photocatalyst. Owing to the creation of a heterojunction between TiO_2 and γ-Fe_2O_3, the photogenerated electrons and holes were divided more effectually and competently. Alternatively, rGO speeded up the carrier mobility at the TiO_2- γ-Fe_2O_3 heterojunction, rising the photogenerated e^-/h^+ separation and thus probably enhancing the photocatalytic performance [21].

2.2. Characterization of 2D MXene based nanocomposites

2.2.1 Structural and morphological analysis of 2D MXene based nanocomposites

In Figure 4a, showed the diffraction pattern of MXene and their composites. The 2θ values of MXene situated at 9.0 and 18.32° corresponding to (0 0 2) and (0 0 4) planes, signifying flourishing MXene preparation. The diffraction peaks of CuO are well-matched with the monoclinic phase of CuO (JCPDS card no: 05-0661). XRD peaks (Fig. 4a) exhibited both phases of MXene and CuO and confirm the formation of MXene/CuO NC, and the peak intensity enhanced with the enlarged CuO content, representing the flourishing preparation of the MXene/CuO NC [23].

The XRD pattern of the hydrothermally prepared NCs (Fig. 4b) showed both phases of hexagonal ZnO and MXene. The planes of hexagonal ZnO and MXene phases are well- matched with the standard JCPDS card no (65-2908 & 52-0875). The ZnO and MXene peaks

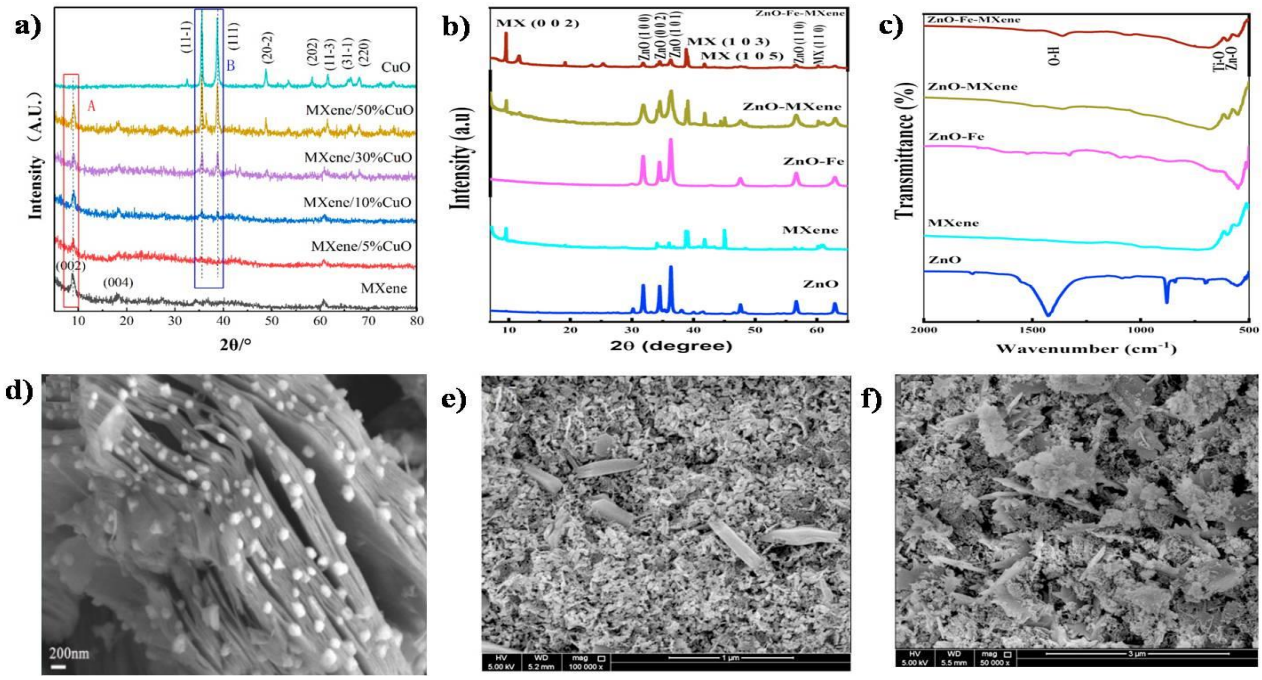

Fig. 4. XRD pattern of (a) MXene/CuO and (b) ZnO-Fe-MXene NC, (c) FTIR spectra of ZnO-Fe-MXene NC, SEM images of (d) MXene/CuO. (e) ZnO-MXene and (c) ZnO-Fe-MXene NC. Reprinted with permission from [Ref. 23, 24].

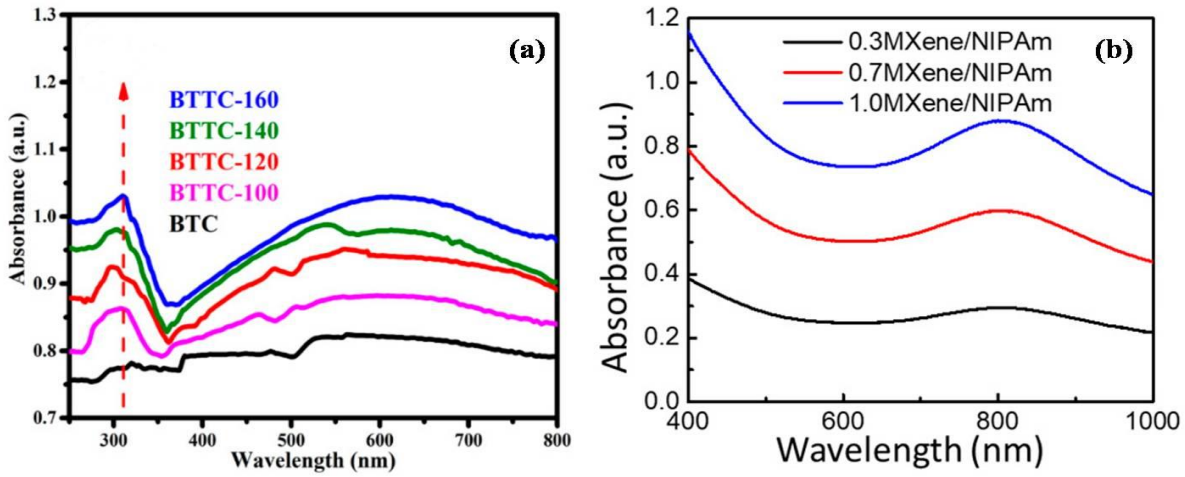

Fig. 5. Absorbance spectra of (a) BTC, BTTC with different calcination temperature (b) MXene/NIPAm sample. Reprinted with permission from [Ref. 25, 26].

display in the ZFM NC and also give the confirmation of NC construction.

The FTIR spectrum acquired for the hydrothermally prepared NCs is illustrated in Figure 4c. This study authenticated the −CH, −OH, and −CO bending and stretching vibrations of the prepared NCs. The peaks are noticed at 1125 and 2922 cm^{-1} due to the bending vibration of the carbonyl group (CO_3^{2-}). The bending and stretching vibrations of hydroxyl groups are situated at 1362 - 3443 cm^{-1}. The peaks at 545 - 600 cm^{-1} are due to the stretching mode Zn–O and Ti–O [24].

Fig. 4d showed the morphology of MXene/50% CuO NC. FESEM images showed the CuO nanoparticles with less than 100 nm were arbitrarily deposited on the Ti_3AlC_2 nanosheets and were stabilized via van der Walls interactions [23].

Fig. 4 e-f exhibited the SEM micrographs of the hydrothermally prepared NCs. From the SEM images, the prepared composites showed a flower-like structure with an average grain size in the range of 100 nm. The inclusion of Fe and MXene emerges a remarkable change in the morphology of ZnO. TiCs is inaccessible on the surface of ZnO that may have embarrassed the development of tiny particles [24].

2.2.2 Optical properties of 2D MXene based nanocomposites

Figure 5a shows the DRS spectra of the prepared BTC and BTTC-x samples. Noticeably, the synthesized BTC discloses the lowest absorption intensity between all the samples, signifying the prepared sample acquires the worst absorption capability in the visible and UV ranges. In correlation, all the prepared BTTC-x samples have better light absorption ability than BTC, signifying that hydrothermal oxidation reaction of titanium carbides is favourable for the enhancement of optical absorption performance. TiO_2 intrinsic light absorption edge at 400 nm can be examined, which is supplied to the emergence of TiO_2 nanoparticles [25].

The UV-Vis spectra (figure 5b) explained a continuing enhance in MXene absorption and also flourishing inclusion into the polymer network (NIPAm). Fig. 5b showed the results corresponding to the MXene on the surface or in immediacy to the interphase [26].

III. 2D based hybrid materials for photocatalytic CO_2 transformation to hydrocarbon fuels

The application of photocatalysis in CO_2 conversion takes part in a noteworthy function to determine the energy crisis and global warming. The development utilizes a light-driven photocatalytic renovation of CO_2 to value-added chemical fuels including CH_4, CO, CH_2O, CH_3OH, and C_2H_5OH. The pure TiO_2, surface tailored TiO_2 and their NCs can be utilized for transforming CO_2 to hydrocarbon fuels, where the creation of C_2H_5OH is two times advanced than that of CH_3OH. The surface tailored TiO_2 showed the CH_3OH and C_2H_5OH production yields are 351 & 134 $\mu mol/g_{cat}h$. The pure TiO_2 showed the CH_3OH and C_2H_5OH production yields are 208 & 143 $\mu mol/g_{cat}h$. From these results, the surface tailored TiO_2 nanomaterials have higher CO_2 transformation activity correlated to the pure TiO_2 nanomaterials [27].

The CH_3OH and C_2H_5OH production yields of the TiO_2/rGO, altered TiO_2/rGO, TiO_2/rGO/CeO_2, and altered TiO_2/rGO/CeO_2 NCs is calculated via photocatalytic transformation method. Among these NCs, the modified TiO_2/rGO/CeO_2 photocatalytic NC displayed the uppermost production yield of CH_3OH and C_2H_5OH (641 and 271 $\mu mol/g_{cat}h$) compared to prepared other NCS. The highest production yield of TiO_2/rGO/CeO_2 photocatalytic NC is due to the optical bandgap of the NC (3.02 eV), multi-step charge transportation, low-electron hole recombination rate, superior specific surface area, high electron mobility and larger interfacial contact area [27].

The photocatalytic CO_2 transformation performance of the TiO_2/Ti_3C_2 (TT550) NC is highlighted. The production rate of CH_4 is 0.22 $\mu mol\ h^{-1}$ by TT550 NC. The prepared TT550 NC production rate was 3.7 times higher than of trade TiO_2 (P25) [28, 38-40]. Additionally,

Table 1

Summary of newly reported 2D based photocatalysts for CO_2 reduction performance

Photocatalyst	Method of synthesis	Light source	CO yield	CH_4 yield	CH_3OH yield	C_2H_5OH yield	Ref.
(Pt/TiO_2) @ rGO	Self assembly	300 W Xe lamp	41.3 μmol $g^{-1}h^{-1}$	0.4 μmol $g^{-1}h^{-1}$	-	-	[29]
Cu_2O/rGO	Microwave-assisted	150 W Xe lamp	46 ppm $g^{-1}h^{-1}$	-	-	-	[30]
rGO-BiO	Hydrothermal route	300 W Xe lamp	4.5 μmol $g^{-1}h^{-1}$	21.75 μmol $g^{-1}h^{-1}$	-	-	[31]
rGO/CuO	Simple chemical method	20 W white cold LED flood light	-	-	1228 μmol $g^{-1}h^{-1}$		[32]
Cu_2O/G/TNA	Electrodeposition	300 W Xe lamp	-	-	45 μmol cm^{-2} h^{-1}	-	[33]
TiO_2/NrGO	Hydrothermal approach	400 W Xe lamp	50 μmol $g^{-1}h^{-1}$	-	-	-	[34]
TiO_2/MoS_2/graphene aerogel (TGM)	Hydrothermal approach	300 W Xe lamp	92.33 μmol $g^{-1}h^{-1}$	-	-	-	[35]
TiO_2/rGO/CeO_2	Ultrasonic-assisted	15 W UC-C mercury lamp	-	-	401 $\mu molg_{cat}h$	147 $\mu molg_{cat}h$	[27]
Modified TiO_2/rGO/CeO_2	Ultrasonic-assisted	15 W UC-C mercury lamp	-	-	641 $\mu molg_{cat}h$	271 $\mu molg_{cat}h$	[27]
$TiO_2/C_3N_4/Ti_3C_2$	Hydrothermal route	350 W Xe lamp	4.39 μmol $g^{-1}h^{-1}$	1.20 μmol $g^{-1}h^{-1}$	-	-	[36]
Ti_3AlC_2	Sonication/self assembly	200 W Hg lamp	0.61 μmol $g^{-1}h^{-1}$	0.05 μmol $g^{-1}h^{-1}$	-	-	[37]
Ti_3AlC_2/TiO_2			2.97 μmol $g^{-1}h^{-1}$	0.59 μmol $g^{-1}h^{-1}$	-	-	[37]
Pg-C_3N_4/ Ti_3AlC_2/TiO_2			4.97 μmol $g^{-1}h^{-1}$	0.64 μmol $g^{-1}h^{-1}$	-	-	[37]

the superior photocatalytic CH_3OH, C_2H_5OH, and CH_4 production performance of the prepared composite with previously reported 2D based hybrid materials (Table 1).

Conclusion and Outlook

It is essential to note here that photocatalytic and electrochemical reduction of carbon dioxide to hydrocarbon fuels is a motivating and impending research area as such; the growth of surprisingly proficient and economical 2D based hybrid catalysts is talented. While, the major attention of this study was to offer photocatalysts that is capable and efficient in transformation of CO_2 into hydrocarbon fuels. This review summarizes the advancement of CO_2 reduction over 2D based hybrid photocatalysts. The appropriate selections of 2D based hybrid material are important in order to achieve the favoured hydrocarbon products such as CH_4, CO, CH_2O, CH_3OH, and C_2H_5OH.

K. Karthik – PhD in Physics, Senior Researcher;
D. Radhika – PhD in Chemistry, Assistant Professor of the Chemistry Department;
D. Gnanasangeetha – PhD in Chemistry, Assistant Professor of the Chemistry Department;
K. Gurushankar – PhD in Physics, Assistant Professor of the Physics Department;
Md Enamul Hoque – PhD in Biomedical Engineering, Professor of the Biomedical Engineering Department.

[1] H. Xu, Y. Li, H. Huang, Spatial research on the effect of financial structure on CO_2 emission Energy Procedia, (Supplement C) 118, 179 (2017) (https://doi.org/10.1016/j.egypro.2017.07.037).
[2] R. Aswini, S. Murugesan, Karthik Kannan, International Journal of Environmental Analytical Chemistry (2020) (DOI: 10.1080/03067319.2020.1718668).
[3] P.V.V. Prasad, J.M.G. Thomas, S. Narayanan, Global warming effects Encyclopaedia of applied plant sciences (second ed.) (Academic Press, Oxford, 2017).
[4] P.M. Cox, R.A. Betts, C.D. Jones, S.A. Spall, I.J. Totterdell, Nature, 408, 184 (2000) (https://doi.org/10.1038/35041539).

[5] Wenjun Zhang, Yi Hu, Lianbo Ma, Guoyin Zhu, Peiyang Zhao, Xiaolan Xue, Renpeng Chen, Songyuan Yang, Jing Ma, Jie Liu, Zhong Jin, Nano Energy 53, 808 (2018) (https://doi.org/10.1016/j.nanoen.2018.09.053).
[6] S. Garg, M. Li, A.Z. Weber, L. Ge, L. Li, V. Rudolph, G. Wang, T.E. Rufford, J Mater Chem A 8, 1511 (2020) (https://doi.org/10.1039/C9TA13298H).
[7] F. Xu, K. Meng, B. Zhu, H. Liu, J. Xu, J. Yu, Adv. Funct. Mater. 29, 1904256 (2019) (https://doi.org/10.1002/adfm.201904256).
[8] C. Bie, B. Zhu, F. Xu, L. Zhang, J. Yu, Adv. Mater. 31, 1902868 (2019) (https://doi.org/10.1002/adma.201902868).
[9] J. Yuan, M.-P. Yang, W.-Y. Zhi, H. Wang, H. Wang, J.-X. Lu, J Carbon Dioxide Util 33, 452 (2019).
[10] Z. Zeng, Y. Yan, J. Chen, P. Zan, Q. Tian, P. Chen, Adv. Funct. Mater. 29, 1806500 (2019) (https://doi.org/10.1002/adfm.201806500).
[11] S. Cao, B. Shen, T. Tong, J. Fu, J. Yu, Adv. Funct. Mater. 28, 1800136 (2018) (https://doi.org/10.1002/adfm.201800136).
[12] Karthik Kannan, D. Radhika, A.S. Nesaraj, Mohammed Wasee Ahmed, R. Namitha, Mater. Res. Innov. 24(7), 414 (2020), (DOI: 10.1080/14328917.2019.1706032).
[13] R. Murugesan, S. Sivakumar, K. Karthik, P. Anandan, M. Haris, Current Applied Physics, 19(10), 1136 (2019) (1144. DOI: 10.1016/j.cap.2019.07.008).
[14] M. Naguib, J. Halim, J. Lu, K. M. Cook, L. Hultman, Y. Gogotsi, and M. W. Barsoum, J. Am. Chem. Soc. 135(43), 15966 (2013) (https://doi.org/10.1021/ja405735d).
[15] D Radhika, Karthik Kannan, A.S Neseraj, R Namitha, Mater. Res. Innov. 24(7), 395 (2020) (401. DOI: 10.1080/14328917.2019.1686858).
[16] M. Naguib, O. Mashtalir, J. Carle, V. Presser, J. Lu, L. Hultman, Y. Gogotsi, M.W. Barsoum, ACS Nano 6(2), 1322 (2012) (https://doi.org/10.1021/nn204153h).
[17] J. Halim, M.R. Lukatskaya, K.M. Cook, J. Lu, C.R. Smith, L.A. Naslund, S.J. May, L. Hultman, Y. Gogotsi, P. Eklund, M.W. Barsoum, Chem. Mater. 26(7), 2374 (2014) (https://doi.org/10.1021/cm500641a).
[18] M. Ghidiu, M. Naguib, C. Shi, O. Mashtalir, L.M. Pan, B. Zhang, J. Yang, Y. Gogotsi, S.J.L. Billinge, and M.W. Barsoum, Chem. Commun. 50(67), 9517 (2014) (https://doi.org/10.1039/C4CC03366C).
[19] Surachet Duanghathaipornsuk, Sushil Kanel, Emily F. Haushalter, Jessica E. Ruetz, Dong-Shik Kim, Nanomaterials 10, 1136 (2020) (https://doi.org/10.3390/nano10061136).
[20] Marin Kovaˇci´c, Klara Perovi´c, Josipa Papac, Antonija Tomi´c, Lev Matoh, Boštjan Žener , Tomislav Brodar, Ivana Capan, Angelja K. Surca, Hrvoje Kuši´c, Urška Lavrenˇciˇc Štangar, Ana Lonˇcari´c Boži´c, Materials 13, 1621 (2020) (https://doi.org/10.3390/ma13071621).
[21] Reyhaneh Kaveh, Maryam Mokhtarifar, Mojtaba Bagherzadeh, Andrea Lucotti, Maria Vittoria Diamanti, MariaPia Pedeferri, Molecules 25, 2996 (2020) (https://doi.org/10.3390/molecules25132996).
[22] Karthik Kannan, Aboubakr M. Abdullah, Kishor Kumar Sadasivuni, Bijandra Kumar, Catalysts 10, 495 (2020) (https://doi.org/10.3390/catal10050495).
[23] Haifeng Zhao, Jing Lv, Junshan Sang, Li Zhu, Peng Zheng, Greg. L. Andrew, Linghua Tan, Materials 11, 2457 (2018) (https://doi.org/10.3390/ma11122457).
[24] Karthik Kannan, Mostafa H. Sliem, Aboubakr M. Abdullah, Kishor Kumar Sadasivuni, Bijandra Kumar Catalysts 10, 549 (2020) (https://doi.org/10.3390/catal10050549).
[25] Ziyu Yao, Huajun Sun, Huiting Sui, Xiaofang Liu, Nanomaterials 10, 452 (2020) (https://doi.org/10.3390/nano10030452).
[26] Sifani Zavahir, Patrik Sobolˇciak, Igor Krupa, Dong Suk Han, Jan Tkac, Peter Kasak, Nanomaterials 10, 1419 (2020) (https://doi.org/10.3390/nano10071419).
[27] Panpailin Seeharaja, Panyata Kongmuna, Piyalak Paiploda, Saowanee Prakobmita, Chaval Sriwonga, Pattaraporn Kim-Lohsoontornb, Naratip Vittayakorn, Ultrasonics - Sonochemistry 58, 104657 (2019) (https://doi.org/10.1016/j.ultsonch.2019.104657).
[28] Jingxiang Low, Liuyang Zhang, Tong Tong, Baojia Shen, Jiaguo Yu, Journal of Catalysis 361, 255 (2018) (https://doi.org/10.1016/j.jcat.2018.03.009).
[29] Y. Zhao, Y. Wei, X. Wu, H. Zheng, Z. Zhao, J. Liu, J. Li, Appl. Catal. B Environ. 226, 360 (2018) (https://doi.org/10.1016/j.apcatb.2017.12.071).
[30] S. Arshadi-Rastabi, J. Moghaddam, M. Reza Eskandarian, J. Ind. Eng. Chem. 22, 34 (2015) (https://doi.org/10.1016/j.jiec.2014.06.022).
[31] S. Sun, M. Watanabe, P. Wang, T. Ishihara, ACS Appl. Energy Mater. 2, 2104 (2019) (https://doi.org/10.1021/acsaem.8b02153).
[32] R. Gusain, P. Kumar, O.P. Sharma, S.L. Jain, O.P. Khatri, Appl. Catal. B Environ. 181, 352 (2016) (https://doi.org/10.1016/j.apcatb.2015.08.012).
[33] F. Li, L. Zhang, J. Tong, Y. Liu, S. Xu, Y. Cao, S. Cao, Nanomater. Energy 27, 320 (2016) (https://doi.org/10.1016/j.nanoen.2016.06.056).
[34] L.Y. Lin, Y. Nie, S. Kavadiya, T. Soundappan, P. Biswas, Chem. Eng. J. 316, 449 (2017) (https://doi.org/10.1016/j.cej.2017.01.125).
[35] H. Jung, K.M. Cho, K.H. Kim, H.-W. Yoo, A. Al-Saggaf, I. Gereige, H.-T. Jung, ACS Sustain. Chem. Eng. 6, 5718 (2018).

[36] Fei He, Bicheng Zhu, Bei Cheng, Jiaguo Yu, Wingkei Ho, Wojciech Macyk, Applied Catalysis B: Environmental 272, 119006 (2020) (https://doi.org/10.1016/j.apcatb.2020.119006).
[37] Muhammad Tahir, Energy Fuels 34, 3540 (2020) (https://doi.org/10.1021/acs.energyfuels.9b04393).
[38] I. Mironyuk, L. Soltys, T. Tatarchuk, V. Tsinurchyn, Physics and Chemistry of Solid State 21(2), 300 (2020) (https://doi.org/10.15330/pcss.21.2.300-311).
[39] N. Danyliuk, T. Tatarchuk, A. Shyichuk, Physics and Chemistry of Solid State 21(4), 727 (2020) (https://doi.org/10.15330/pcss.21.4.727-736).
[40] N. Danyliuk, T. Tatarchuk, A. Shyichuk, Physics and Chemistry of Solid State 21(2), 338 (2020) (https://doi.org/10.15330/pcss.21.2.338-346).

К. Картік[1], Д. Радхіка[2], Д. Гнанасангіта[3], К. Гурушанкар[4.5], Мд Енамул Хоге[6]

Двовимірні гібридні матеріали для фотокаталітичного перетворення вуглекислого газу у вуглеводневі палива: міні-огляд

[1]Школа передового матеріалознавства та інженерії, Національний технологічний інститут Кумох, Гумі, Південна Корея, karthikkannanphotochem@gmail.com
[2]Хімічний факультет, Школа інженерії та технологій, університет Джейн, Карнатака, Індія, radhikadv8@gmail.com
[3]Хімічний факультет, PSNA Інженерний коледж в Котхандарамані Нагар, Тамілнад, Індія, sangithprakash@psnacet.edu.in
[4]Вища школа медицини та біології, Південно-Уральський державний університет, Челябінськ, Росія.
[5]Фізичний факультет, Школа передових наук, Академія досліджень та освіти Каласалінгам, Тамілнад, Індія, gurushankar01051987@gmail.com
[6]Факультет біомедичної інженерії, Військовий науково-технологічний інститут, Дхака, Бангладеш, enamul1973@gmail.com

Перетворення вуглекислого газу в хімічні речовини та паливо на основі двовимірних гібридних матеріалів є сьогодні важливим питанням для ґрунтовних обговорень у фізиці, хімії та електрохімії за новими та важливими галузями матеріалознавства, енергетики та екологічної стійкості. Величезні можливості для двовимірних гібридних матеріалів в області фотокаталітичного перетворення вуглекислого газу виникають завдяки широким можливостям їх застосування. У галузі перетворення вуглекислого газу наноструктуровані оксиди металу з двовимірною композитною системою матеріалу повинні відповідати гарантованим конструктивним та функціональним критеріям, а також відповідним електричним та механічним властивостям. Відповідно, запропонований огляд базується на вивчених на цей час даних про синтез двовимірних наноматеріалів, оксиду металу із композитами, вимог щодо перетворення вуглекислого газу, використання двовимірних матеріалів з нанокомпозитами при перетворенні вуглекислого газу, як палива та основні механізми, задіяні при цьому. Також обговорено вплив гібридних матеріалів та синергетичних композиційних сумішей, які широко використовуються або мають перспективи в області фотокаталітичного перетворення вуглекислого газу.

Ключові слова: 2D-наноматеріали; характеристика; фотокаталітичне перетворення вуглекислого газу; паливо.